STABILITY ANALYSIS OF ARBITRARY-LAGRANGIAN-EULERIAN ADER-DG METHODS ON CLASSICAL AND DEGENERATE SPACETIME GEOMETRIES*

MAURO BONAFINI†, DAVIDE TORLO‡, AND ELENA GABURRO§

Abstract. In this paper, we present a thorough von Neumann stability analysis of explicit and implicit Arbitrary-Lagrangian-Eulerian (ALE) ADER discontinuous Galerkin (DG) methods on *classical* and *degenerate* spacetime *geometries* for hyperbolic equations.

First, we rigorously study the CFL stability conditions for the *explicit* ADER-DG method, confirming results widely used in the literature while specifying their limitations. Moreover, we highlight under which conditions on the mesh velocity the ALE methods, constrained to a given CFL, are actually stable.

Next, we extend the stability study to ADER-DG in the presence of *degenerate spacetime elements*, with *zero size* at the beginning and the end of the time step, but with a *non zero spacetime volume*. This kind of elements has been introduced in a series of articles on direct ALE methods by Gaburro *et al.* to connect via spacetime control volumes regenerated Voronoi tessellations after a topology change. Here, we imitate this behavior in 1d by fictitiously inserting degenerate elements in between two cells. Then, we show that over this degenerate spacetime geometry, both for the explicit and implicit ADER-DG, the *CFL stability constraints remain the same* as those for classical geometries, laying the theoretical foundations for their use in the context of ALE methods.

Key words. Von Neumann stability analysis, CFL stability constraints, Arbitrary-Lagrangian-Eulerian methods, ADER discontinous Galerkin methods, explicit and implicit high order methods, degenerate spacetime geometries

MSC codes. 65M12, 65M60, 35L02, 65M50.

1. Introduction.

The spacetime predictor-corrector ADER approach, introduced in its original formulation in [53, 71], extended to nonlinear systems in [72, 70] and to unstructured domains in [40, 39, 19, 10], and finally presented with a modern and effective approach in [16], is nowadays widely used to reach high order of accuracy also in time when solving hyperbolic partial differential equations (PDEs). It consists of an element-local iterative method to construct a piece-wise polynomial, called predictor, that represents an approximation of high order of accuracy both in space and time of the PDE solution. Then, in the corrector phase, the predictor is directly inserted into a one-step update formula to evolve the solution from one time step to the next one. The method has been shown to be very reliable and effective since it introduces minimal dissipation and can be parallelized with minimal communication overhead [25, 18].

In particular, ADER approaches can be used within the framework of discontinuous Galerkin (DG) finite element methods, as originally proposed in [62, 20, 45, 34]. Later, the ADER-DG methods have been applied to many different hyperbolic systems, starting from the classical Euler and shallow water equations [63, 26, 66, 14], multiphase models [66, 41], magnetohydrodynamics [2, 24], dispersive, turbulent and

*Submitted to the editors DATE.

Funding: This work was funded by the ERC Starting Grant *ALcHyMiA* (grant agreement No. 101114995). Further details can be found in the Acknowledgments Section.

†Department of Computer Science, University of Verona, Strada le Grazie 15, Verona, 37134, Italy (mauro.bonafini@univr.it).

‡Mathematics Department "Guido Castelnuovo", University of Rome Sapienza, p.le Aldo Moro, 5, Rome, 00189, Italy. (davide.torlo@uniroma1.it).

§Department of Computer Science, University of Verona, Strada le Grazie 15, Verona, 37134, Italy (elena.gaburro@univr.it).

reactive flows [9, 76, 8, 58], up to the study of much more complex systems, as unified models for continuum mechanics [21, 22, 69, 7, 13, 42] and various first order reformulations of the Einstein field equations for general relativity [23, 77, 54].

Over the years, many authors have worked with ADER-DG schemes proposing performance improvements [35, 50, 73, 59, 47], implicit [17] and semi-implicit [56, 6, 61] formulations, and in particular their use in the context of *direct* Arbitrary-Lagrangian-Eulerian (ALE) methods [5]. In this latter framework, the mesh moves following as close as possible the local fluid flow and, in order to evolve the PDE from one mesh to the next one, an effective approach consists in connecting them via space-time control volumes, eventually degenerate [30, 31, 29], over which integrating the PDE. Here, ADER-DG methods offer the ideal tools to build a one-step solver that is automatically able to integrate the PDE in space and time and to perform *directly* the time update (without any need for projection and reconstruction procedures, typical of *indirect* approaches [46, 3]).

Given the widespread adoption of ADER and ADER-DG methods, a rigorous theoretical investigation of their fundamental properties becomes necessary. While the convergence of the local spacetime predictor has been established for linear problems in [38] and extended to nonlinear systems in [7], stability studies still require further investigation. Regarding stability, some authors have addressed ADER-type schemes in the simplified framework of ordinary differential equations [36, 61, 60], but a comprehensive analysis in the PDE setting is still missing. The seminal work [16] provides stability considerations only for low polynomial degrees, while for higher orders the admissible CFL numbers are typically determined empirically. Moreover, to the best of our knowledge, no dedicated analysis has been carried out for the newly introduced ALE ADER-DG methods on possibly degenerate spacetime geometries.

For the above reasons, it is of general interest to establish a rigorous stability analysis of ADER-DG methods. There are several strategies to study the stability of numerical methods, some of which apply only to linear problems, while others are also able to treat nonlinear problems. For linear problems, one can look at the Lax–Richtmyer stability [43], which, however, turns out to be difficult to prove in many situations. In the context of periodic domains, the von Neumann stability analysis guarantees Lax–Richtmyer stability and can be easily performed using Fourier modes instead of fully discretized problems, strongly reducing the complexity of the stability analysis. Indeed, there are many works that have studied the von Neumann stability to deduce CFL conditions or other parameter conditions, e.g. for residual distribution in 1d and 2d [51, 52] and for DG in 1d [68].

The extension of linear analyses to nonlinear problems is not straightforward, but the results obtained in the linear setting are often a good indicator of the CFL that should be used in the presence of non linearities. A direct study of the L^2 stability can be done also in the non linear case, but it would still require an analysis of all the degrees of freedom and it is typically easy to apply only to simple time discretization (explicit/implicit Euler, SSPRK) [15, 44]. Another way to tackle the stability would be to mimic the integration by parts at the discrete level to guarantee energy or entropy stability in the spatial discretization [27, 55], and also to apply relaxation in time to preserve or dissipate a global entropy [64, 1, 33].

1.1. Aim and structure of this paper. The scope of this paper is to fill the theoretical gap in ADER-DG methods by providing a thorough von Neumann stability analysis, accounting for both the explicit and implicit formulations on fixed or moving meshes. In Section 2, to fix the notation and to make the paper self-consistent, we

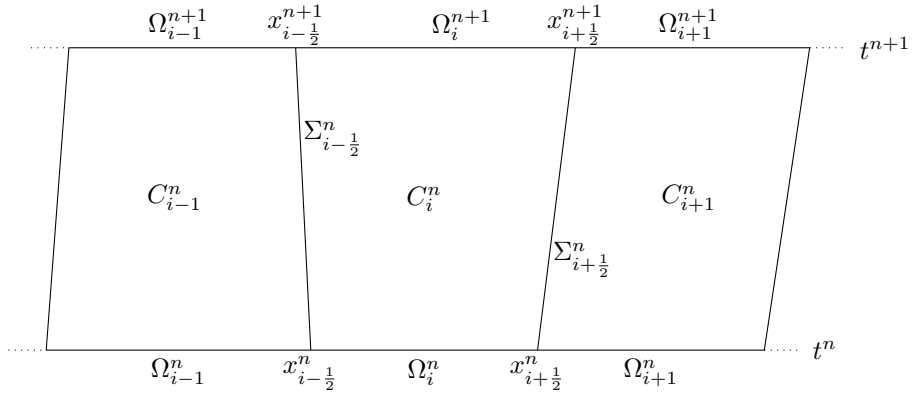

Fig. 1: Prototype configuration of a classical space-time domain discretization.

present the ADER-DG scheme written in the so-called direct Arbitrary-Lagrangian-Eulerian framework. We apply it to scalar nonlinear hyperbolic PDEs on a classical 1d+time geometry. Next, in Section 3, we perform the von Neumann stability analysis of the method and show numerical results for its consistency order. Then, in Section 4, we introduce into our computational domain *fictitious spacetime degenerate elements* that mimic the behavior of the hole-like sliver elements used in [30, 28, 31, 29] to connect meshes with topology changes, and we study the stability and consistency of the method in their presence. Finally, in Section 5, we draw our conclusions and we provide an outlook on future developments.

2. Explicit and implicit formulation of ALE ADER-DG methods. Let us consider a first order nonlinear scalar hyperbolic PDE

$$\partial_t Q(x,t) + \partial_x f(Q(x,t)) = 0, \tag{2.1}$$

where Q denotes the conserved scalar variable and f denotes the flux function.

Geometry description. Given an initial domain $\Omega^0 = [x_L, x_R]$, with $x_L, x_R \in \mathbb{R}$, we consider $N_e + 1$ points $x_L = x_{1/2}^0 < x_{3/2}^0 < \cdots < x_{N_e+1/2}^0 = x_R$ and define N_e spatial elements $\Omega_i^0 := [x_{i-1/2}^0, x_{i+1/2}^0]$, $i = 1, \ldots, N_e$. Given an initial time $t^0 \in \mathbb{R}$, we discretize time by means of intervals $[t^n, t^{n+1}]$ with $n \in \mathbb{N}$ of step size $\Delta t^n = t^n - t^{n-1} > 0$ for $n > 0$. When not ambiguous, we will simply use the notation Δt for Δt^n. In a Lagrangian perspective, we also assume the spatial computational domain to depend on t: at each time t^n our computational domain is then denoted as $\Omega^n = [x_L^n, x_R^n]$, and we consider again N_e+1 points $x_L^n = x_{1/2}^n < x_{3/2}^n < \cdots < x_{N_e+1/2}^n = x_R^n$ and define N_e elements $\Omega_i^n := [x_{i-1/2}^n, x_{i+1/2}^n]$, $i = 1, \ldots, N_e$. We denote the length of each element by $\Delta x_i^n := |\Omega_i^n| = (x_{i+1/2} - x_{i-1/2})$ and define its barycentre $b_i^n := (x_{i+1/2} + x_{i-1/2})/2$. For each $i = 1, \ldots, N_e$, we also define $\Sigma_{i\pm1/2}$ as the segment connecting $(x_{i\pm1/2}^n, t^n)$ to $(x_{i\pm1/2}^{n+1}, t^{n+1})$ and introduce the spacetime control volume C_i^n as the polygonal set with vertices $(x_{i-1/2}^n, t^n), (x_{i+1/2}^n, t^n), (x_{i+1/2}^{n+1}, t^{n+1}), (x_{i-1/2}^{n+1}, t^{n+1})$. In particular, $\partial C_i^n = \Sigma_{i-1/2}^n \cup (\Omega_i^n \times \{t^n\}) \cup \Sigma_{i+1/2}^n \cup (\Omega_i^{n+1} \times \{t^{n+1}\})$. We refer to Figure 1 for a visual depiction of the setting.

Families of basis functions. We fix a polynomial degree $N > 0$. For each $n > 0$ and $i \in \{1, \dots, N_e\}$, we introduce three different sets of basis functions. First, we define over each domain Ω_i^n the set of *spatial* basis functions $\{\phi_{i,\ell}^n\}_\ell$, which are defined as

$$\phi_{i,\ell}^n \colon \Omega_i^n \to \mathbb{R},\ x \mapsto \left(\frac{x - b_i^n}{\Delta x_i^n}\right)^\ell \quad \text{for } \ell = 0, \dots, N. \tag{2.2}$$

Next, we define over each spacetime control volume two different sets of basis functions: the set of *spacetime* basis functions $\{\theta_{i,\ell}^n\}_\ell$, defined as

$$\begin{aligned} &\theta_{i,\ell}^n \colon C_i^n \to \mathbb{R},\ (x,t) \mapsto \left(\frac{x - b_i^n}{\Delta x_i^n}\right)^{\ell_1} \left(\frac{t - t^n}{\Delta t}\right)^{\ell_2} \\ &\text{for } \ell = \ell_1 + (\ell_1 + \ell_2)(\ell_1 + \ell_2 + 1)/2,\ 0 \le \ell_1 + \ell_2 \le N, \\ &\text{so that } \ell = 0, \dots, N_{st} - 1, \text{ with } N_{st} := (N+1)(N+2)/2, \end{aligned} \tag{2.3}$$

and the set of *moving* basis functions $\{\psi_{i,\ell}^n\}_\ell$, defined as

$$\begin{aligned} &\psi_{i,\ell}^n \colon C_i^n \to \mathbb{R},\ (x,t) \mapsto \left(\frac{x - \tilde{b}_i^n(t)}{\Delta x_i^n}\right)^\ell \quad \text{for } \ell = 0, \dots, N, \\ &\text{with } \ \tilde{b}_i^n(t) = \left(1 - \frac{t - t^n}{\Delta t}\right) b_i^n + \frac{t - t^n}{\Delta t} b_i^{n+1}. \end{aligned} \tag{2.4}$$

Representation of the approximate solution. The conserved variable Q is represented over each grid element Ω_i^n via a piecewise polynomial function u_i^n in the form

$$u_i^n(x) = \sum_{\ell=0}^{N} \phi_{i,\ell}^n(x)\, \hat{u}_{i,\ell}^n \quad \text{for } x \in \Omega_i^n,\ i \in \{1, \dots, N_e\}, n > 0, \tag{2.5}$$

where $\{\hat{u}_{i,\ell}^n\}_{n,i,\ell} \subset \mathbb{R}$ are the degrees of freedom. We also write $\hat{u}_i^n \in \mathbb{R}^{N+1}$ to identify the corresponding vector of coefficients. The family $\{u_i^n\}_i$ defines a global (discontinuous) approximant u^n over Ω^n, which is well-defined everywhere except at the interfaces between elements. Approximations defined on each control volume C_i^n will usually take the form of a spacetime polynomial function q_i^n written as

$$q_i^n(x,t) = \sum_{\ell=0}^{N_{st}-1} \theta_{i,\ell}^n(x,t) \hat{q}_{i,\ell}^n, \quad \text{for } (x,t) \in C_i^n,\ i \in \{1, \dots, N_e\}, n > 0, \tag{2.6}$$

where $\{\hat{q}_{i,\ell}^n\}_{n,i,\ell} \subset \mathbb{R}$ are the degrees of freedom. Again, we write $\hat{q}_i^n \in \mathbb{R}^{N_{st}}$ to identify the corresponding vector of coefficients.

2.1. Explicit ALE ADER-DG method.

Given an approximate solution u^n in the form (2.5), the explicit ALE ADER-DG method is a two steps method aiming to compute the next approximant u^{n+1}. These steps are termed *predictor* and *corrector* step.

2.1.1. Predictor step. The aim of this step is to build a *local* approximation of the governing PDE (2.1) over each spacetime control volume C_i^n, using u_i^n as initial condition at time t^n. We seek over each spacetime control volume C_i^n, $i = 1, \dots, N_e$, a spacetime polynomial function q_i^n of the form (2.6) whose coefficients $\hat{q}_i^n$ are to be determined so that q_i^n solves the element-local Cauchy problem

$$\begin{cases} \partial_t q_i^n(x,t) + \partial_x f(q_i^n(x,t)) = 0 & \text{over } C_i^n, \\ q_i^n(x,t^n) = u_i^n(x) & \text{on } \Omega_i^n. \end{cases}$$

We fix now any spacetime test function $\theta_{i,k}^n$, $k = 0, \dots, N_{st} - 1$, multiply the above PDE by $\theta_{i,k}^n$ and integrate over the given control volume C_i^n to get

$$\int_{C_i^n} \theta_{i,k}^n(x,t) \left[\partial_t q_i^n(x,t) + \partial_x f(q_i^n(x,t))\right] dxdt = 0 \quad \text{for } k = 0, \dots, N_{st} - 1. \tag{2.7}$$

Then, we rewrite the first term in (2.7) by taking into account a potential jump of q_i^n at the boundary Ω_i^n of C_i^n via a simplified path-conservative approach [57, 12, 11], obtaining

$$\begin{aligned} &\int_{C_i^n} \theta_{i,k}^n(x,t) \partial_t q_i^n(x,t)\, dxdt + \int_{\Omega_i^n} \theta_{i,k}^n(x,t^n)\, \left(q_i^n(x,t^n) - u_i^n(x)\right)\, dx \\ &\quad + \int_{C_i^n} \theta_{i,k}^n(x,t) \partial_x f(q_i^n(x,t))\, dxdt = 0 \qquad \text{for } k = 0, \dots, N_{st} - 1. \end{aligned} \tag{2.8}$$

For a given q_i^n, we now define the vector $\hat{f}_i^n = (\hat{f}_{i,0}^n, \dots, \hat{f}_{i,N_{st}-1}^n)$ so that

$$f_i^n(x,t) = \sum_{\ell=0}^{N_{st}-1} \theta_{i,\ell}^n(x,t) \hat{f}_{i,\ell}^n \qquad \begin{array}{l} \text{is the } L^2\text{-projection of } f(q_i^n) \text{ over the finite} \\ \text{dimensional space span}\{\theta_{i,0}^n, \dots, \theta_{i,N_{st}-1}^n\}. \end{array} \tag{2.9}$$

Finally, by replacing in (2.8) the term $f(q_i^n)$ with f_i^n, we get

$$\begin{aligned} &\int_{C_i^n} \theta_{i,k}^n(x,t) \partial_t q_i^n(x,t)\, dxdt + \int_{\Omega_i^n} \theta_{i,k}^n(x,t^n) q_i^n(x,t^n)\, dx \\ &= \int_{\Omega_i^n} \theta_{i,k}^n(x,t^n) u_i^n(x)\, dx - \int_{C_i^n} \theta_{i,k}^n(x,t) \partial_x f_i^n(x,t)\, dxdt \\ &\text{for } k = 0, \dots, N_{st} - 1. \end{aligned} \tag{2.10}$$

By expanding q_i^n and u_i^n in (2.10), see (2.6) and (2.5), we obtain an implicit system of equations for the unknown coefficient vector $\hat{q}_i^n$. Here, the coefficient vector $\hat{f}_i^n$ is indeed a (generally nonlinear) function of $\hat{q}_i^n$, and so to approximate $\hat{q}_i^n$ we employ a fixed point Picard iteration, as detailed in [16, 37, 7]. We can consider the vector $\hat{q}_i^{n,(0)} := (\hat{u}_{i,0}^n, \dots, \hat{u}_{i,N}^n, 0, \dots, 0)$ as starting point for the iteration and remark that such fixed point procedure has already been proved to be convergent and to yield the desired order of accuracy, see [38, 7, 36] for more details.

Upon convergence, the predictor step provides us with a set of locally defined high-order polynomials q_i^n over each control volume C_i^n. These polynomials will serve as approximant of the solution in the interior of C_i^n and will be used in the computation of the numerical fluxes at the interfaces.

2.1.2. Corrector step. For each $i \in \{1, \dots, N_e\}$, we multiply the governing equation (2.1) by a moving basis function $\psi^n_{i,k}$, $k = 0, \dots, N$, and integrate over the control volume C^n_i to obtain

$$\int_{C^n_i} \psi^n_{i,k}(x,t) \left[\partial_t Q(x,t) + \partial_x f(Q(x,t))\right] dxdt = 0 \quad \text{for } k = 0, \dots, N.$$

Next, by integration by parts, we get

$$\int_{\partial C^n_i} \psi^n_{i,k}(Q\, \hat{n}^n_{i,t} + f(Q)\, \hat{n}^n_{i,x})\, ds - \int_{C^n_i} \partial_t \psi^n_{i,k} Q + \partial_x \psi^n_{i,k} f(Q)\, dxdt = 0 \quad \text{for } k = 0, \dots, N,$$

where $\hat{\mathbf{n}}^n_i = (\hat{n}^n_{i,x}, \hat{n}^n_{i,t})$ denotes the outward pointing unit normal vector on the space-time faces composing the boundary ∂C^n_i. We now decompose ∂C^n_i into Ω^n_i, Ω^{n+1}_i and the two lateral faces $\Sigma^n_{i\pm 1/2}$, we recall that u^n_i (resp. u^{n+1}_i) approximates Q on Ω^n_i (resp. Ω^{n+1}_i) and that the predictor q^n_i approximates Q inside the control volume C^n_i. Upon introducing a suitable numerical flux function $\mathcal{F} \colon \mathbb{R} \times \mathbb{R} \times S^1 \to \mathbb{R}$, we obtain

$$\begin{aligned} &\int_{\Omega^{n+1}_i} \psi^n_{i,k}(x, t^{n+1}) u^{n+1}_i(x)\, dx = \int_{\Omega^n_i} \psi^n_{i,k}(x, t^n) u^n_i(x)\, dx \\ &- \int_{\Sigma^n_{i-\frac{1}{2}}} \psi^n_{i,k} \mathcal{F}(q^n_i, q^n_{i-1}, \hat{\mathbf{n}}^n_i)\, ds - \int_{\Sigma^n_{i+\frac{1}{2}}} \psi^n_{i,k} \mathcal{F}(q^n_i, q^n_{i+1}, \hat{\mathbf{n}}^n_i)\, ds \\ &+ \int_{C^n_i} \partial_t \psi^n_{i,k}(x,t) q^n_i(x,t) + \partial_x \psi^n_{i,k}(x,t) f(q^n_i(x,t))\, dxdt \quad \text{for } k = 0, \dots, N, \end{aligned} \tag{2.11}$$

where the coefficient vector $\hat{u}^{n+1}_i$ can be computed *explicitly* upon knowing $\hat{u}^n_i$ and by integrating the remaining terms that depend only on the already computed predictors q^n_i. The above formula is termed the *corrector* step of the ADER-DG scheme.

The numerical flux function $\mathcal{F}$ is computed via an ALE Riemann solver applied to the inner and outer boundary-extrapolated data q^- and q^+ at each boundary. Here, the simplest choice consists in adopting a Rusanov-type [67] ALE flux: for $q^-, q^+ \in \mathbb{R}$ and $\hat{\mathbf{n}} = (\hat{n}_x, \hat{n}_t) \in S^1$, we set

$$\mathcal{F}(q^-, q^+, \hat{\mathbf{n}}) = \frac{1}{2}\left(f(q^+) + f(q^-)\right)\hat{n}_x + \frac{1}{2}\left(q^+ + q^-\right)\hat{n}_t - \frac{1}{2} s_{\max}\left(q^+ - q^-\right), \tag{2.12}$$

where, in full generality, $s_{\max}$ is the maximum of the spectral radii of the ALE Jacobian matrix w.r.t. the normal direction in space evaluated at q^- and q^+, which here simplifies to

$$s_{\max} = \max\{|f'(q^-) - v|, |f'(q^+) - v|\} \cdot |\hat{n}_x|,$$

where $v = -\hat{n}_t/|\hat{n}_x|$ is the local grid velocity. For the general expression for systems and in higher dimension we refer to [4].

2.2. Implicit ALE ADER-DG method. Opposite to the explicit method, the implicit ALE ADER-DG method directly seeks a *global* approximant q^n by means of simultaneously computing all approximants q^n_i over each control volume C^n_i. For each $i \in \{1, \dots, N_e\}$, we multiply the governing equation (2.1) by a spacetime basis function $\theta^n_{i,k}$, $k = 0, \dots, N_{st} - 1$, and integrate over the control volume C^n_i to obtain

$$\int_{C^n_i} \theta^n_{i,k}(x,t) \left[\partial_t Q(x,t) + \partial_x f(Q(x,t))\right] dxdt = 0 \quad \text{for } k = 0, \dots, N_{st} - 1.$$

Next, by integration by parts, we get

$$\int_{\partial C_i^n} \theta_{i,k}^n (f(Q),Q)\cdot \hat{\mathbf{n}}_i^n \, ds - \int_{C_i^n} \partial_t \theta_{i,k}^n Q + \partial_x \theta_{i,k}^n f(Q)\, dxdt = 0 \quad \text{for } k = 0,\dots,N_{st}-1,$$

where $\hat{\mathbf{n}}_i^n = (\hat{n}_{i,x}^n, \hat{n}_{i,t}^n)$ denotes the outward pointing spacetime unit normal. Now, on each control volume C_i^n we substitute Q by an approximant q_i^n in the form (2.6), we decompose the boundary integral into four integrals (one over each of the four faces), we introduce a suitable numerical flux $\mathcal{F}$ and require $q_i^n(x,t^n) = u_i^n(x)$ for $x \in \Omega_i^n$, to get

$$\begin{aligned}
&\int_{\Omega_i^{n+1}} \theta_{i,k}^n(x,t^{n+1}) q_i^n(x,t^{n+1})\, dx - \int_{C_i^n} \partial_t \theta_{i,k}^n(x,t) q_i^n(x,t)\, dxdt \\
&- \int_{C_i^n} \partial_x \theta_{i,k}^n(x,t) f_i^n(x,t)\, dxdt + \int_{\Sigma_{i-\frac{1}{2}}^n} \theta_{i,k}^n \mathcal{F}(q_i^n, q_{i-1}^n, \hat{\mathbf{n}}_i^n)\, ds \\
&+ \int_{\Sigma_{i+\frac{1}{2}}^n} \theta_{i,k}^n \mathcal{F}(q_i^n, q_{i+1}^n, \hat{\mathbf{n}}_i^n)\, ds = \int_{\Omega_i^n} \theta_{i,k}^n(x,t^n) u_i^n(x)\, dx \\
&\text{for } i = 1,\dots,N_e \text{ and } k = 0,\dots,N_{st}-1,
\end{aligned} \tag{2.13}$$

where f_i^n is defined as in (2.9). The set of equations (2.13) implicitly defines a generally nonlinear system for the coefficients $\{\hat{q}_{i,\ell}^n\}_{i,\ell}$, which we solve by means of a Newton iteration coupled with a GMRES algorithm. Once each q_i^n has been computed, the next approximant u_i^{n+1} can be recovered through an L^2 projection of $q_i^n(\cdot,t^{n+1})$ with respect to the basis $\{\phi_{i,\ell}^{n+1}\}_\ell$.

3. Stability of ALE ADER-DG methods on classical geometries. We move now to the focus of this paper. We are interested in studying the stability of the explicit ADER-DG method introduced in Section 2 by means of the well known von Neumann stability analysis technique [43, Chapters 9.6 and 10.5]. Hence, we consider the linear advection equation (LAE) for a constant advection velocity $a > 0$, so that $f(Q) = aQ$. We restrict ourselves to the domain $\Omega = [0, 2\pi]$ and consider a uniform grid of N_e elements of size $\Delta x > 0$ and a positive Δt. For a given wave number $\kappa \in \mathbb{N}$, we consider the periodic initial condition $u_0(x) = e^{\mathrm{i}\kappa x}$ and close the system with periodic boundary conditions. Since the initial condition satisfies $u_0(x-\Delta x) = e^{-\mathrm{i}\kappa\Delta x} u_0(x)$ for every $x \in \mathbb{R}$, it can be easily proved that the coefficients generated by an ADER-DG method on a fixed grid satisfy $\hat{u}_{i-1}^n = e^{-\mathrm{i}\kappa\Delta x}\hat{u}_i^n$ for any i, n (with the appropriate modifications at the boundaries).

3.1. Stability of the explicit method. To describe the explicit ADER-DG as applied to this setting, we first observe that we can drop the dependency of basis functions from the individual elements, since each Ω_i^n can be obtained (up to translation) from the interval $[0,1]$ rescaled by Δx and each control volume C_i^n from the cube $[0,1]\times[0,1]$ rescaled by Δx in space and by Δt in time. We conveniently define the reference basis functions

$$\begin{aligned}
\phi_\ell \colon [0,1] \to \mathbb{R},\ \xi \mapsto (\xi - 1/2)^\ell \quad &\text{for } \ell = 0,\dots,N, \\
\psi_\ell \colon [0,1]\times[0,1] \to \mathbb{R},\ (\xi,\tau) \mapsto \phi_\ell(\xi) \quad &\text{for } \ell = 0,\dots,N,
\end{aligned}$$

and

$$\begin{aligned}
&\theta_\ell \colon [0,1]\times[0,1] \to \mathbb{R},\ (\xi,\tau) \mapsto (\xi-1/2)^{\ell_1}\ \tau^{\ell_2} \\
&\text{for } \ell = \ell_1 + (\ell_1+\ell_2)(\ell_1+\ell_2+1)/2,\ 0 \le \ell_1+\ell_2 \le N.
\end{aligned}$$

Since $f(Q) = aQ$, each predictor step in (2.10) simplifies to

$$\hat{q}_i^n = \left(K_\tau^{st} + K_0^{st} + \frac{a\Delta t}{\Delta x} K_\xi^{st} \right)^{-1} M_0 \hat{u}_i^n, \tag{3.1}$$

where the three $N_{st} \times N_{st}$ matrices $K_\tau^{st}, K_0^{st}, K_\xi^{st}$ and the $N_{st} \times (N+1)$ matrix M_0 are defined as

$$\begin{aligned} [K_\tau^{st}]_{k,\ell} &= \int_0^1 \int_0^1 \theta_k \partial_t \theta_\ell \, dxdt, & [K_\xi^{st}]_{k,\ell} &= \int_0^1 \int_0^1 \theta_k \partial_x \theta_\ell \, dxdt, \\ [K_0^{st}]_{k,\ell} &= \int_0^1 \int_0^1 \theta_k \theta_\ell \, dxdt, & [M_0]_{k,\ell} &= \int_0^1 \theta_k(x,0) \phi_\ell(x) \, dx. \end{aligned} \tag{3.2}$$

By taking now into account that the Rusanov-type flux (2.12) for the LAE is a simple upwind scheme and recalling $a > 0$, the subsequent corrector step in (2.11) simplifies to

$$\hat{u}_i^{n+1} = \hat{u}_i^n + \frac{a\Delta t}{\Delta x} M^{-1} (K_\xi \hat{q}_i^n - F_-^r \hat{q}_i^n + F_-^l \hat{q}_{i-1}^n), \tag{3.3}$$

where the three $(N+1) \times N_{st}$ matrices K_ξ, F_-^r, F_-^l and the $(N+1) \times (N+1)$ mass matrix M are defined as

$$\begin{aligned} [M]_{k,\ell} &= \int_0^1 \phi_k \phi_\ell \, dx, & [K_\xi]_{k,\ell} &= \int_0^1 \partial_x \psi_k \theta_\ell \, dxdt, \\ [F_-^r]_{k,\ell} &= \int_0^1 \psi_k(x,1) \theta_\ell(x,1) \, dx, & [F_-^l]_{k,\ell} &= \int_0^1 \psi_k(x,0) \theta_\ell(x,1) \, dx. \end{aligned} \tag{3.4}$$

Since $\hat{u}_{i-1}^n = e^{-\mathrm{i}\kappa\Delta x} \hat{u}_i^n$, we have from (3.1) that $\hat{q}_{i-1}^n = e^{-i\kappa\Delta x} \hat{q}_i^n$. Hence, the update in (3.3) reduces to

$$\begin{aligned} \hat{u}_i^{n+1} &= \hat{u}_i^n + \frac{a\Delta t}{\Delta x} M^{-1} (K_\xi - F_-^r + e^{-\mathrm{i}\kappa\Delta x} F_-^l) \hat{q}_i^n \\ &= \hat{u}_i^n + \frac{a\Delta t}{\Delta x} M^{-1} (K_\xi - F_-^r + e^{-\mathrm{i}\kappa\Delta x} F_-^l) \left(K_\tau^{st} + K_0^{st} + \frac{a\Delta t}{\Delta x} K_\xi^{st} \right)^{-1} M_0 \hat{u}_i^n \\ &= A(\mathrm{CFL}, \theta) \cdot \hat{u}_i^n, \end{aligned}$$

with an amplification matrix $A(\mathrm{CFL}, \theta) \in \mathbb{R}^{(N+1)\times(N+1)}$ dependent only on $\theta = \kappa\Delta x$ and $\mathrm{CFL} = a\Delta t/\Delta x$. For a matrix A, let us denote by $\rho(A)$ its spectral radius. Then, for a given CFL number, the update formula for $\hat{u}_i^n$ is stable, regardless of the value of Δx, if and only if

$$\max_{\theta \in [0, 2\pi]} \rho(A(\mathrm{CFL}, \theta)) \leq 1. \tag{3.5}$$

Study of the stability condition. For each $N = 1, \ldots, 9$, we compute analytically the matrices in (3.2), (3.4), and we build the matrix $A(\mathrm{CFL}, \theta)$. First, we observe that the method always preserves constant states: indeed, for $\theta = 0$ and $\hat{u}_i^n = (1, 0, \ldots, 0)$, we have $A(\mathrm{CFL}, 0) \cdot \hat{u}_i^n = \hat{u}_i^n$, independently on CFL. Hence, we know that the maximum in (3.5) is always at least 1. Now we numerically study the stability condition in

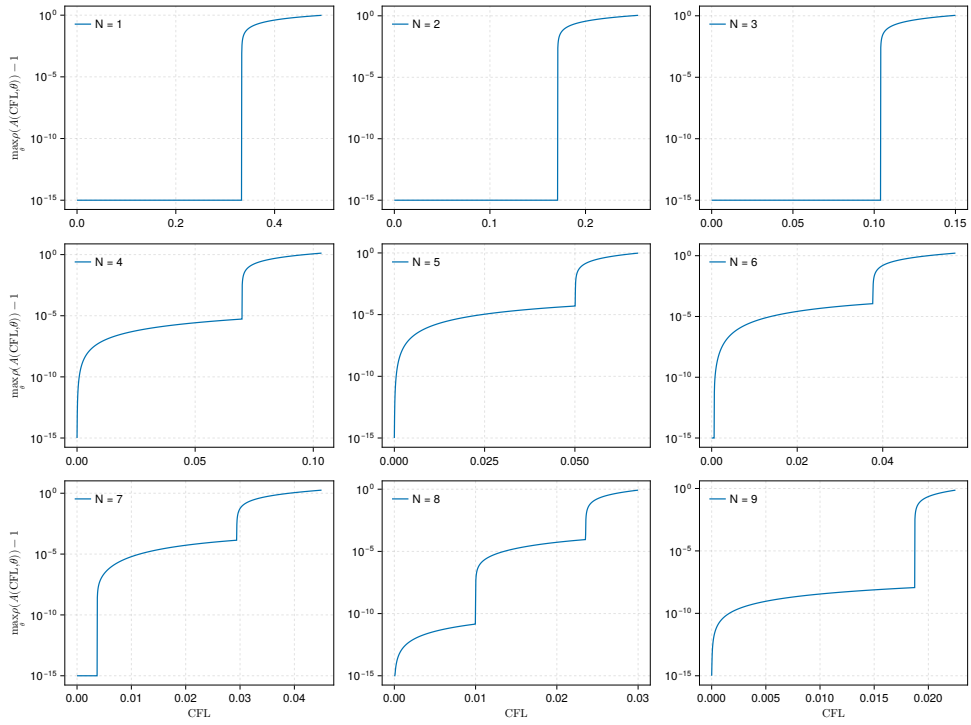

Fig. 2: Semi-logarithmic plot of the function CFL $\mapsto \max_\theta \rho(A(\mathrm{CFL}, \theta)) - 1$, which guarantees stability of explicit ADER-DG whenever it vanishes, see (3.5).

(3.5) by taking the maximum over the set of 1001 equispaced $\theta \in [0, 2\pi]$. By looking at Figure 2, we identify the following relevant values for the CFL:

(3.6)

N	1	2	3	4	5	6	7	8	9
CFL	0.333	0.170	0.104	0.069	0.050	0.037	0.029	0.023	0.018

For $N \leq 3$, the method is stable for CFL numbers lower than those reported in Table (3.6), in accordance with the analysis in [16]. On the other hand, for $4 \leq N \leq 9$, the method turns out to be unstable for the reported CFL values. These numbers just correspond to the rightmost jump in each plot, where the stability condition, even if only slightly, is violated. Stability can be recovered for much smaller values of the CFL number, as shown in Figure 3.

We remark that the CFL values reported in Table (3.6), even if they do not correspond to true stability limits, are consistent with those widely used in the community (see, e.g., [32, 13, 65]), which have generally been determined empirically. By a matter of facts, in complex test cases, the small amplification factor due to instability is mitigated when combined with other discretization techniques such as numerical viscosity, Riemann solvers, damping factors, and limiters. As a result, authors usually adopt these values as their reference maximum CFL number when running numerical experiments.

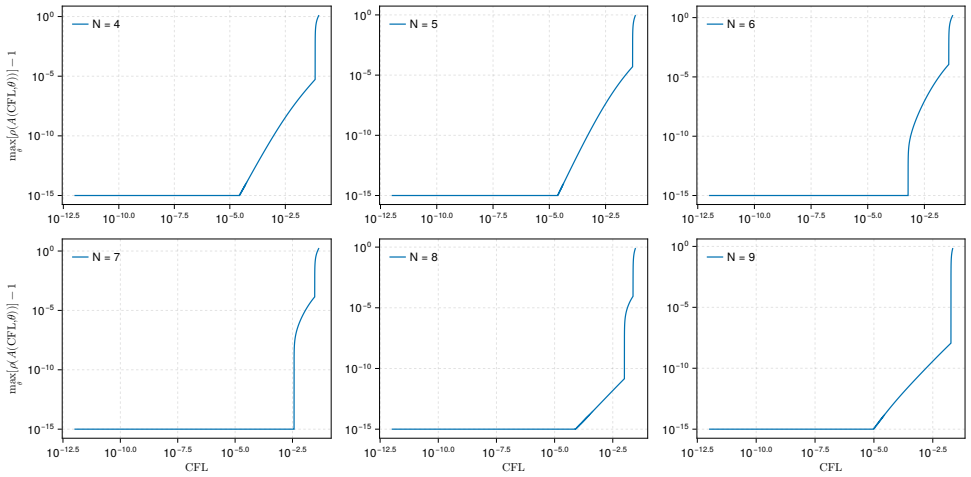

Fig. 3: Logarithmic plot of the function $\mathrm{CFL} \mapsto \max_\theta \rho(A(\mathrm{CFL}, \theta)) - 1$.

Remark 3.1. The analysis extends to the case of a mesh moving with uniform velocity $v \in \mathbb{R}$. In this context, the stability condition turns into

$$|a - v| \frac{\Delta t}{\Delta x} \leq \mathrm{CFL}_{\max}.$$

Assuming $a > 0$, by using a value $\tilde{c} \leq \mathrm{CFL}_{\max}$ and selecting $\Delta t = \tilde{c}\Delta x/a$, the condition above rewrites as

$$a\left(1 - \frac{\mathrm{CFL}_{\max}}{\tilde{c}}\right) \leq v \leq a\left(1 + \frac{\mathrm{CFL}_{\max}}{\tilde{c}}\right),$$

which provides a bound on the admissible velocities of the grid. For example, if $\tilde{c} = \mathrm{CFL}_{\max}$ one obtains $0 \leq v \leq 2a$, while if $\tilde{c} = 0.5 \cdot \mathrm{CFL}_{\max}$ the condition becomes $-a \leq v \leq 3a$, allowing more freedom in the mesh velocities.

3.2. Numerical consistency order of the explicit method. The explicit ADER-DG method is expected to have order of consistency $N+1$ for a given polynomial degree N. We verify this property by evolving a linear advection equation with unit velocity on the domain $[-6, 6]$, with periodic boundary conditions and starting from $Q(x, 0) = e^{-x^2}$. We vary the number of elements N_e and we consider $\Delta t = 0.9 \cdot \mathrm{CFL}_{\max} \cdot \Delta x$, where $\Delta x = 12/N_e$ and $\mathrm{CFL}_{\max}$ is taken from Table (3.6). In the top pictures of Figure 4, we report, in logarithmic scale, the L^2 norm of the error with respect to the exact solution at time $T = 1$. Each consistency order is correctly achieved.

3.3. Stability of the implicit method. The stability analysis for the implicit ADER-DG method can be developed following the same steps used for the explicit counterpart. Again, we have to study the spectral radius of a suitable amplification matrix $A(\mathrm{CFL}, \theta)$, which can be computed exactly. Condition (3.5) is numerically satisfied, up to machine precision, for a fine sample of CFL numbers within the interval $[0, 10]$ and for every $N = 1, \ldots, 9$, thereby confirming that the scheme is unconditionally stable (as proved in [17]).

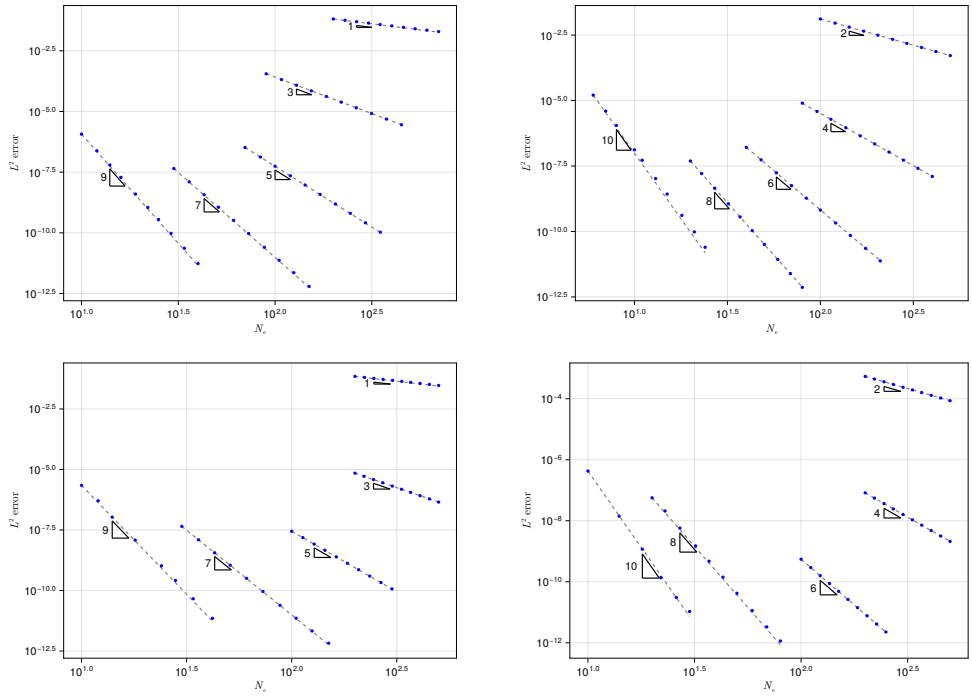

Fig. 4: Consistency order of explicit (top) and implicit (bottom) ADER-DG: left odd orders for $N = 0, 2, 4, 6, 8$, right even orders for $N = 1, 3, 5, 7, 9$.

3.4. Numerical consistency order on classical geometries. The implicit ADER-DG method, as its explicit counterpart, is expected to have order of consistency $N+1$ for a given polynomial degree N. We verify this property by means of the same LAE evolution test case described in Section 3.2, where now we consider a global $\mathrm{CFL}_{\max} = 0.2$, independently of the degree N. Again, by looking at the bottom pictures of Figure 4, each consistency order is correctly achieved.

4. ALE ADER-DG methods on degenerate spacetime geometries. In this section, we consider a modification of the ALE ADER-DG scheme on degenerate spacetime geometries, which are obtained by introducing in our computational domain *fictitious spacetime degenerate elements*, which will be termed *sliver* elements.

Geometry description. To construct a *degenerate* spacetime geometry we start from the classical geometry described in Figure 1. As in Figure 6, we assume now that some of the interfaces $\Sigma^n_{i-1/2}$ are expanded into a *sliver element* $S^n_{i-1/2}$, which represents our fictitious spacetime degenerate element. To construct a sliver element $S^n_{i-1/2}$, we first fix its maximal width $\Delta x^n_{i-1/2} > 0$ and then consider the quadrilateral whose vertices, in counter-clockwise order, are defined as

$$(x^n_{i-1/2}, t^n), \qquad ((x^n_{i-1/2} + x^{n+1}_{i-1/2} + \Delta x^n_{i-1/2})/2, t^n + \Delta t/2),$$
$$(x^{n+1}_{i-1/2}, t^{n+1}), \quad ((x^n_{i-1/2} + x^{n+1}_{i-1/2} - \Delta x^n_{i-1/2})/2, t^n + \Delta t/2).$$

Each neighbouring control volume is redefined accordingly. The boundary $\partial S^n_{i-1/2}$ of

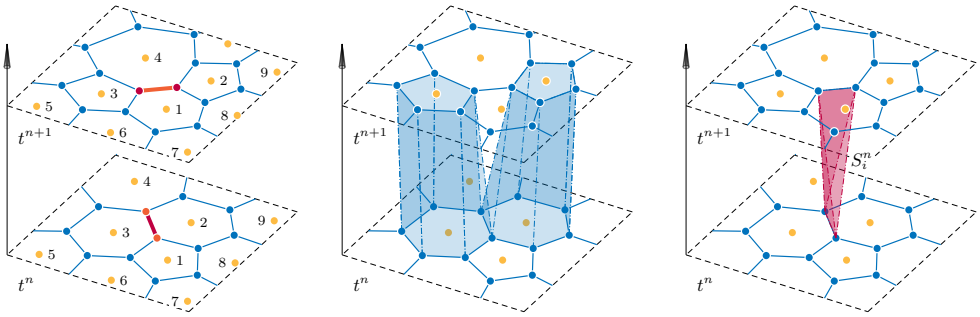

Fig. 5: Spacetime connectivity with topology changes in 2d (left), induced hole-like sliver element (right) and neighbouring classical control volumes (middle).

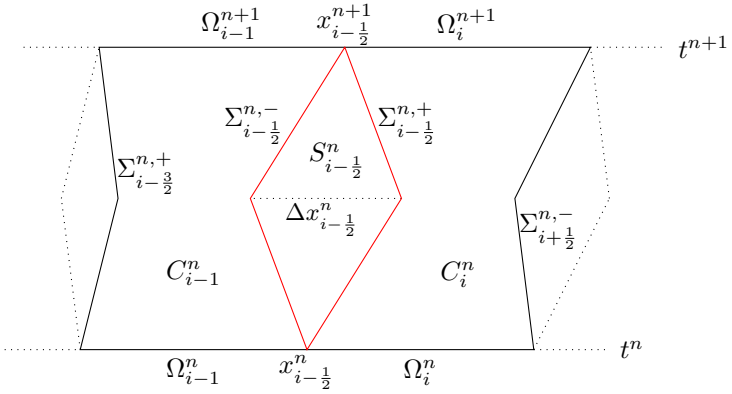

Fig. 6: Prototype configuration of a space-time domain discretization with a degenerate (or sliver) element.

each sliver element can be viewed as the union of $\Sigma_{i-1/2}^{n,-}$ (the interface between $S_{i-1/2}^n$ and C_{i-1}^n) and $\Sigma_{i-1/2}^{n,+}$ (the interface between $S_{i-1/2}^n$ and C_i^n). In case an interface $\Sigma_{i-1/2}^n$ is not replaced by a sliver element, then we set $\Sigma_{i-1/2}^{n,\pm} := \Sigma_{i-1/2}^n$.

Remark 4.1. These degenerate elements mimic in 1d the hole-like sliver elements introduced in [30, 31, 28, 29] within the framework of 2d moving meshes with topology changes, see Figure 5. Those works are all based on the use of a direct ALE approach for the evolution of the PDE and therefore on the integration over control volumes that connect in time two different meshes. When, in this context, the meshes do not merely move but can also change topology, meaning that connectivity and list of neighbours of each cell may change, the use of classical control volumes to connect the meshes is no longer sufficient. To cover the entire spacetime domain in between, it then becomes necessary to introduce additional volumes, such as those shown in the right panel of Figure 5, which, similarly to the 1d degenerate elements of this paper, have zero area at both times t^n and t^{n+1}, but a non zero spacetime volume. At present, the 2d sliver elements have been used in a variety of applications, but a theoretical analysis of their properties has not yet been carried out in detail.

Basis functions. For each $n > 0$ and $i \in \{1, \dots, N_e\}$, we consider the already introduced families of basis functions $\{\phi^n_{i,\ell}\}_\ell$, $\{\theta^n_{i,\ell}\}_\ell$ and $\{\psi^n_{i,\ell}\}_\ell$, see (2.2), (2.3) and (2.4). Furthermore, we also consider over each sliver element $S^n_{i-1/2}$ the family of *spacetime* basis function $\{\theta^n_{i-1/2,\ell}\}_\ell$ defined as

$$\theta^n_{i-\frac{1}{2},\ell} \colon S^n_{i-\frac{1}{2}} \to \mathbb{R},\ (x,t) \mapsto \left(\frac{x - x^n_{i-\frac{1}{2}}}{\Delta x^n_{i-\frac{1}{2}}}\right)^{\ell_1} \left(\frac{t-t^n}{\Delta t}\right)^{\ell_2}$$
$$\text{for } \ell = \ell_1 + (\ell_1+\ell_2)(\ell_1+\ell_2+1)/2,\ 0 \le \ell_1 + \ell_2 \le N,$$

Alongside the general approximants u^n_i and q^n_i described in (2.5) and (2.6), we also consider approximants defined on each sliver element $S^n_{i-1/2}$ to take the form of a spacetime polynomial function $q^n_{i-1/2}$ written as

$$q^n_{i-\frac{1}{2}}(x,t) = \sum_{\ell=0}^{N_{st}-1} \theta^n_{i-\frac{1}{2},\ell}(x,t)\hat{q}^n_{i-\frac{1}{2},\ell}, \text{ for } (x,t) \in C^n_{i-\frac{1}{2}},\ i \in \{2,\dots,N_e\}, n > 0, \tag{4.1}$$

where $\{\hat{q}^n_{i-1/2,\ell}\}_{n,i,\ell} \subset \mathbb{R}$ are the degrees of freedom. Again, we write $\hat{q}^n_{i-1/2}$ to identify the corresponding vector of coefficients.

4.1. Explicit ALE ADER-DG on degenerate geometries.

The explicit ALE ADER-DG scheme on degenerate geometries can be describe as a three steps scheme, where the third additional step is devoted to the treatment of the newly introduced sliver elements.

Predictor step on control volumes. The predictor step of the explicit ALE ADER-DG scheme on non-degenerate control volumes remains essentially the same as the one described in Section 2.1.1. The only difference is the possible non-quadrilateral concave structure of some control volumes C^n_i that should be accounted during the numerical integration. Thus, we can easily apply (2.10) to obtain each predictor q^n_i, $i = 1, \dots, N_e$.

Predictor step on sliver elements. Once predictors on non-degenerate control volumes are computed, we consider the sliver elements. Let us fix a sliver element $S^n_{i-1/2}$ for some $i \in \{2, \dots, N_e\}$. Since we have no inflow information to work with at time t^n (due to the sliver degeneracy) on such elements, we perform a complete integration by parts that allows to introduce inflow boundary conditions through flux exchanges at the interfaces $\Sigma^{n,\pm}_{i-1/2}$. Hence, we follow the same derivation that led to (2.13) and we seek for an approximant $q^n_{i-1/2}$ of the form (4.1) that solves

$$\begin{aligned} &\int_{\Sigma^{n,-}_{i-\frac{1}{2}}} \theta^n_{i-\frac{1}{2},k} \mathcal{F}(q^n_{i-\frac{1}{2}}, q^n_{i-1}, \hat{\mathbf{n}}^n_{i-\frac{1}{2}})\, ds + \int_{\Sigma^{n,+}_{i+\frac{1}{2}}} \theta^n_{i-\frac{1}{2},k} \mathcal{F}(q^n_{i-\frac{1}{2}}, q^n_i, \hat{\mathbf{n}}^n_{i-\frac{1}{2}})\, ds \\ &= \int_{S^n_{i-\frac{1}{2}}} \partial_t \theta^n_{i-\frac{1}{2},k}(x,t) q^n_{i-\frac{1}{2}}(x,t) + \partial_x \theta^n_{i-\frac{1}{2},k}(x,t) f^n_{i-\frac{1}{2}}(x,t)\, dxdt \\ &\quad \text{for } k = 0, \dots, N_{st}-1, \end{aligned} \tag{4.2}$$

where $f^n_{i-1/2}$ is defined as in (2.9) (by replacing the indices accordingly) and $\hat{\mathbf{n}}^n_{i-1/2}$ is the outward pointing normal to $\partial S^n_{i-1/2}$. By taking into account that predictors on the neighbouring non-degenerate control volumes have already been computed, we can approximate the only unknown $\hat{q}^n_{i-1/2}$ in equation (4.2) by means of a Picard

fixed point iteration initialized by a constant approximant defined by the average of the neighbouring values.

Corrector step. On each element Ω_i^{n+1}, $i = 1, \dots, N_e$, the new approximant u_i^{n+1} is then computed by means of (2.11), with the needed substitutions of predictors and interfaces whenever the control volume neighbours a sliver element. We remark that no additional computations are required on sliver elements because they have zero measure boundary at time t^{n+1}. Moreover, the method is conservative by construction also around sliver elements thanks to the exchange of fluxes already performed in the computation of their predictors: indeed, the balance of the fluxes can be obtained by taking $\theta^n_{i-1/2,0} = 1$ as test function in (4.2).

4.2. Implicit ALE ADER-DG on degenerate geometries. To recover the implicit version of the ALE ADER-DG scheme on degenerate geometries, it is enough to consider together (2.13) on non-degenerate elements and (4.2) on sliver elements, by paying attention to use the correct neighbours and interfaces in (2.13). Again, each new approximant u_i^{n+1} is then recovered by means of an L^2 projection of $q_i^n(\cdot, t^{n+1})$ with respect to the basis $\{\phi_{i,\ell}^{n+1}\}_\ell$.

4.3. Von Neumann stability analysis with spacetime hole-like sliver elements. The von Neumann stability analysis can be performed in the same fashion as outlined in Section 3. Again, we consider an initial data of the form $e^{\mathrm{i}\kappa x}$.

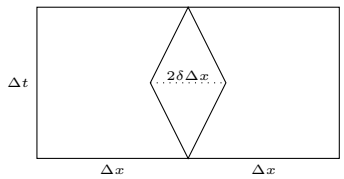

We build our domain starting from a classical Eulerian geometry and replace every other vertical interface with a sliver like element, whose diameter is controlled by a parameter $\delta \in [0, 0.5]$. Now, we identify two subsequent elements $i-1$ and i separated by a sliver to be our unitary periodic block. The geometry is described in the sketch on the side.

Explicit method. We study the update of the couple $\hat{v}_i^n = (\hat{u}_{i-1}^n, \hat{u}_i^n)$, which encodes the coefficients of the approximated solution on the given block. While the derivation is somehow cumbersome, we can easily prove that the vector $\hat{v}_i^n \in \mathbb{R}^{2(N+1)}$ follows an update rule of the form

$$\hat{v}_i^{n+1} = A(\mathrm{CFL}, \delta, \theta) \cdot \hat{v}_i^n,$$

with an amplification matrix $A(\mathrm{CFL}, \delta, \theta) \in \mathbb{R}^{2(N+1)\times 2(N+1)}$ dependent only on $\theta = \kappa\Delta x$, the parameter δ controlling the width of the sliver and $\mathrm{CFL} = a\Delta t/\Delta x$. Thus, for a fixed couple (CFL, δ), the update formula for $\hat{v}_i^n$ is stable, regardless of the value of Δx, if and only if

$$\max_{\theta\in[0,2\pi]} \rho(A(\mathrm{CFL}, \delta, \theta)) \leq 1. \tag{4.3}$$

We perform a numerical study of condition (4.3) in Figure 7. We note that for δ close to 0 the maximal allowed CFL reduces to the one studied in Section 3, as one would expect. But even more interestingly, we remark that increasing δ does not lead to a different behaviour, allowing us to conclude that the introduction of the sliver elements does not change the stability properties of the original method.

Implicit method. The same von Neumann stability analysis can be developed for the implicit ADER-DG method, by focusing again on the update formula for the couple $\hat{v}_i^n = (\hat{u}_{i-1}^n, \hat{u}_i^n)$. The method turns out to be numerically stable for all values of $N \in \{1, \dots, 9\}$, $\mathrm{CFL} \in (0, 10)$ and $\delta \in (0, 0.5)$ that have been tested. Indeed,

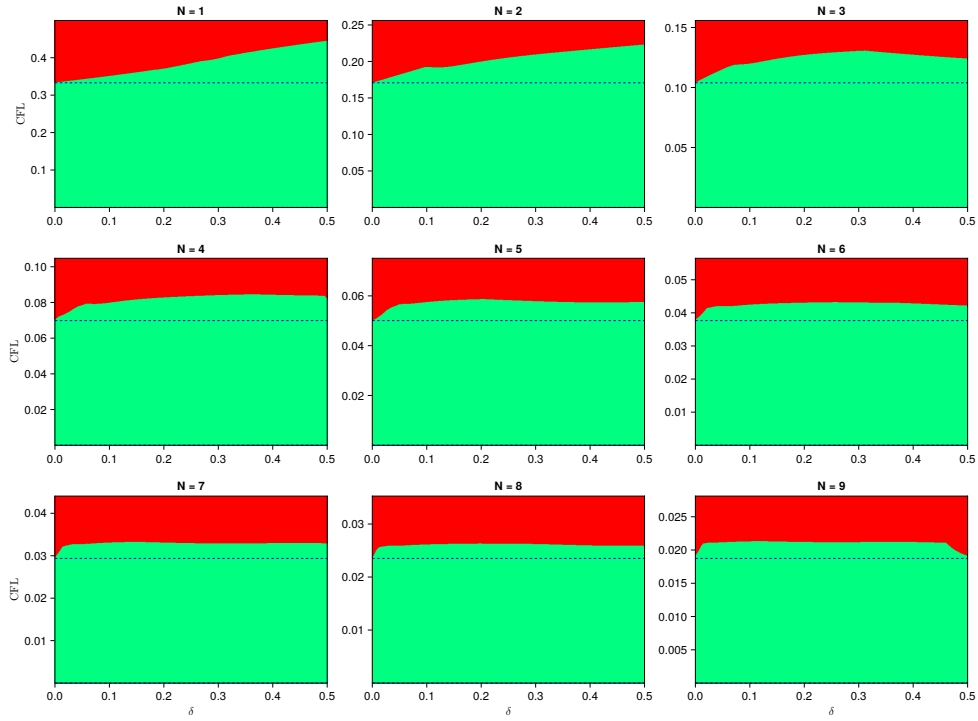

Fig. 7: Stability study of explicit ADER-DG method with slivers. The blue dotted lines are set at the $\mathrm{CFL}_{\max}$ values reported in Table (3.6). Then, in each plot, a point (δ, CFL) is either green or red depending on whether $\max_\theta \rho(A(\mathrm{CFL}, \delta, \theta)) \leq 1 + \varepsilon_N$, where ε_N is the left value at the rightmost jump in the corresponding plot in Figure 2. We deduce that classical CFL numbers can be used even in presence of sliver elements.

following the same idea outlined in the stability proofs in [17, 74, 75], we can actually prove that the method is L^2 stable in some configurations of interest.

THEOREM 4.2 (Stability for implicit ADER-DG with slivers). *On a linear advection equation $\partial_t u + \partial_x u = 0$, the implicit ADER-DG method on a degenerate geometry with $\delta \leq \frac{1}{2} \min\left\{\frac{\Delta t}{\Delta x}, 1\right\}$ is L^2 stable.*

Proof. We recall the construction in Figure 6.

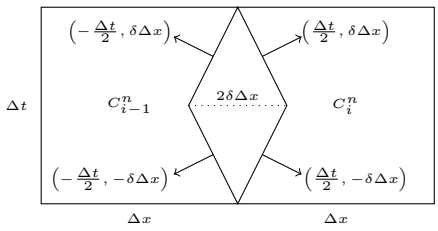

We consider again a periodic degenerate geometry where one every other interface is replaced by a sliver element. We focus on a triplet of elements $(C^n_{i-1}, S^n_{i-1/2}, C^n_i)$, with $\delta \in (0, 0.5)$. Up to renormalization, the normals to the four inner sides of the sliver have the coordinates reported in the picture on the side.

First, we observe that under the assumption $f(q) = q$, the Rusanov-type ALE flux

(2.12) can be simplified into

$$\mathcal{F}(q^-, q^+, \hat{\mathbf{n}}) = \frac{1}{2}\left[(q^+ + q^-)(\hat{\mathbf{n}}_x + \hat{\mathbf{n}}_t) - (q^+ - q^-)|\hat{\mathbf{n}}_x + \hat{\mathbf{n}}_t|\right],$$

meaning that either q^+ or q^- is selected depending on the sign of $(\hat{\mathbf{n}}_x + \hat{\mathbf{n}}_t)$. In particular, given that $\delta \leq \frac{1}{2}\frac{\Delta t}{\Delta x}$, in the subsequent steps the numerical flux will always select q_{i-1} when evaluated along $\Sigma^{n,-}_{i-1/2}$ and $q^n_{i-1/2}$ when evaluated along $\Sigma^{n,+}_{i-1/2}$, resulting into a pure upwind scheme from the left to the right element.

For given continuous spacetime functions u, v and for all meaningful indices i, n, we define for convenience the following pairings:

$$[w,v]^n_i := \int_{\Omega^n_i} w(x,t^n)v(x,t^n)\,dx, \quad \{w,v\}^n_{i-1/2} := \int_{t^n}^{t^{n+1}} w(x_{i-1/2},t)v(x_{i-1/2},t)\,dt,$$

$$\langle w,v\rangle^n_i := \int_{C^n_i} w(x,t)v(x,t)\,dxdt, \quad \langle w,v\rangle^n_{i-1/2} := \int_{S^n_{i-1/2}} w(x,t)v(x,t)\,dxdt,$$

$$\{w,v\}^{n,\pm}_{i-1/2} := \int_{\Sigma^{n,\pm}_{i-1/2}} wv(\mathbf{n}_t + \mathbf{n}_x)\,ds \quad \text{where } \mathbf{n} \text{ is the outer normal to } \partial S^n_{i-1/2}.$$

Consider now (2.13) on the element C^n_i: by recalling that we obtained each initial status as $u^n_i(x) = q^{n-1}_i(x,t^n)$ for $x \in \Omega^n_i$, plugging in as test function q^n_i itself into (2.13), we obtain

$$[q^n_i, q^n_i]^{n+1}_i - [q^n_i, q^{n-1}_i]^n_i - \langle \partial_t q^n_i + \partial_x q^n_i, q^n_i\rangle^n_i - \{q^n_i, q^n_{i-1/2}\}^{n,+}_{i-1/2} + \{q^n_i, q^n_i\}^n_{i+1/2} = 0.$$

By using that $\partial_t((q^n_i)^2) = 2q^n_i\partial_t q^n_i$ and $\partial_x((q^n_i)^2) = 2q^n_i\partial_x q^n_i$, and applying the divergence theorem, we get

$$\begin{aligned}&[q^n_i, q^n_i]^{n+1}_i - [q^n_i, q^{n-1}_i]^n_i - \frac{1}{2}[q^n_i, q^n_i]^{n+1}_i + \frac{1}{2}[q^n_i, q^n_i]^n_i\\ &+ \frac{1}{2}\{q^n_i, q^n_i\}^{n,+}_{i-1/2} - \frac{1}{2}\{q^n_i, q^n_i\}^n_{i+1/2} - \{q^n_i, q^n_{i-1/2}\}^{n,+}_{i-1/2} + \{q^n_i, q^n_i\}^n_{i+1/2} = 0.\end{aligned}$$

By multiplying by 2, adding and subtracting $[q^{n-1}_i, q^{n-1}_i]^n_i$ and $\{q^n_{i-1/2}, q^n_{i-1/2}\}^{n,+}_{i-1/2}$, and rearranging the terms, we obtain

$$\begin{aligned}&[q^n_i, q^n_i]^{n+1}_i - [q^{n-1}_i, q^{n-1}_i]^n_i + [q^n_i - q^{n-1}_i, q^n_i - q^{n-1}_i]^n_i + \{q^n_i, q^n_i\}^n_{i+1/2}\\ &+ \{1, (q^n_i - q^n_{i-1/2})^2\}^{n,+}_{i-1/2} - \{q^n_{i-1/2}, q^n_{i-1/2}\}^{n,+}_{i-1/2} = 0.\end{aligned}$$

Given our choice of δ, we can easily see that $\{1, (q^n_i - q^n_{i-1/2})^2\}^{n,+}_{i-1/2} \geq 0$, hence, from the equality above, we get the inequality

$$[q^n_i, q^n_i]^{n+1}_i - [q^{n-1}_i, q^{n-1}_i]^n_i + \{q^n_i, q^n_i\}^n_{i+1/2} - \{q^n_{i-1/2}, q^n_{i-1/2}\}^{n,+}_{i-1/2} \leq 0. \tag{4.4}$$

Consider now the sliver element $S^n_{i-1/2}$ and the corresponding relation (4.2): by using as test function $q^n_{i-1/2}$ itself, we readily obtain

$$-\langle \partial_t q^n_{i-1/2} + \partial_x q^n_{i-1/2}, q^n_{i-1/2}\rangle^n_{i-1/2} + \{q^n_{i-1/2}, q^n_{i-1/2}\}^{n,+}_{i-1/2} + \{q^n_{i-1/2}, q^n_{i-1}\}^{n,-}_{i-1/2} = 0.$$

By applying again the divergence theorem to the first term, multiplying by 2, adding and subtracting $\{q^n_{i-1}, q^n_{i-1}\}^{n,-}_{i-1/2}$ and rearranging the terms, we derive

$$\{q^n_{i-1/2}, q^n_{i-1/2}\}^{n,+}_{i-1/2} - \{1, (q^n_{i-1/2} - q^n_{i-1})^2\}^{n,-}_{i-1/2} + \{q^n_{i-1}, q^n_{i-1}\}^{n,-}_{i-1/2} = 0.$$

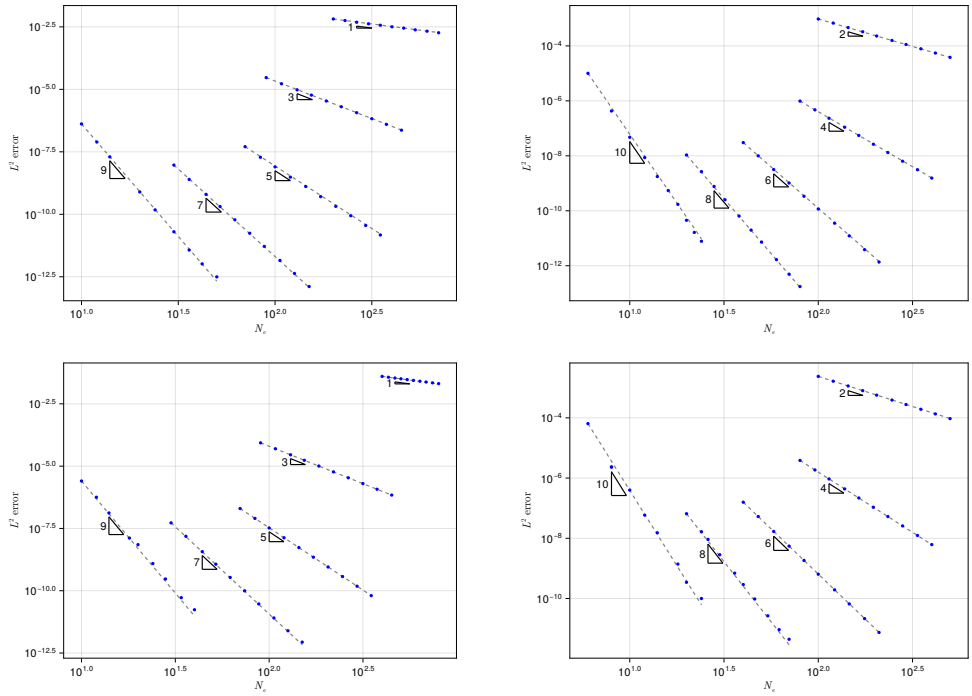

Fig. 8: Consistency order of explicit (top) and implicit (bottom) ADER-DG method with slivers: left odd orders for $N = 0, 2, 4, 6, 8$, right even orders for $N = 1, 3, 5, 7, 9$.

By our choice of δ, we have $\{1, (q^n_{i-1/2} - q^n_{i-1})^2\}^{n,-}_{i-1/2} \leq 0$, leading to

$$\{q^n_{i-1/2}, q^n_{i-1/2}\}^{n,+}_{i-1/2} + \{q^n_{i-1}, q^n_{i-1}\}^{n,-}_{i-1/2} \leq 0. \tag{4.5}$$

On the left element C^n_{i-1}, the same derivation done on C^n_i applies, and we obtain

$$[q^n_{i-1}, q^n_{i-1}]^{n+1}_{i-1} - [q^{n-1}_{i-1}, q^{n-1}_{i-1}]^n_{i-1} - \{q^n_{i-1}, q^n_{i-1}\}^{n,-}_{i-1/2} - \{q^n_{i-2}, q^n_{i-2}\}^n_{i-3/2} \leq 0. \tag{4.6}$$

By taking the sum of (4.4), (4.5) and (4.6), we get

$$\begin{aligned}&[q^n_i, q^n_i]^{n+1} - [q^{n-1}_i, q^{n-1}_i]^n + [q^n_{i-1}, q^n_{i-1}]^{n+1} - [q^{n-1}_{i-1}, q^{n-1}_{i-1}]^n \\ &+ \{q^n_i, q^n_i\}^n_{i+1/2} - \{q^n_{i-2}, q^n_{i-2}\}^n_{i-3/2} \leq 0.\end{aligned}$$

We sum now over all positive indices i and over time, by assuming zero inflow/outflow conditions at the boundary, and obtain

$$\int_\Omega (q^n(x, t^{n+1}))^2 - (q^0(x, 0))^2 \, dx \leq 0,$$

which concludes the proof. ∎

4.4. Numerical consistency with spacetime hole-like sliver elements. As both the explicit and the implicit ADER-DG method on degenerate geometries are derived as generalizations of the ones on classical geometries, we expect them to

also have order of consistency $N+1$ for a given polynomial degree N. To verify this property we repeat the same numerical analysis of Sections 3.2 and 3.4, over a domain where we insert a sliver element at each interface (except at the boundary), with $\delta = 0.2$. In Figure 8, we report L^2 errors with respect to the exact solution at time $T = 1$ in logarithmic scale. Each consistency order is correctly achieved.

5. Conclusions and outlook to future works. In this paper, we studied the von Neumann stability and the consistency of the family of ADER-DG methods for $N = 1, \dots, 9$, considering both explicit and implicit formulations, all within the ALE framework. In particular, we showed that the use of degenerate spacetime geometries is subject to the same stability constraints of those governing stability in the case of classical geometries. Therefore, elements with zero spatial size do not lead to a reduction of the time step. This result is also important because it provides a theoretical foundation for the use of degenerate elements to connect moving meshes in multiple dimensions, and it represents a natural starting point for the construction of new spacetime cut cell-based methods [48, 49].

Acknowledgments. M. Bonafini is member of the INdAM GNAMPA group in Italy; D. Torlo and E. Gaburro are members of the INdAM GNCS group in Italy. E. Gaburro and M. Bonafini gratefully acknowledge the support received from the European Union with the ERC Starting Grant *ALcHyMiA* (grant agreement No. 101114995). Views and opinions expressed are however those of the author only and do not necessarily reflect those of the European Union or the European Research Council Executive Agency. Neither the European Union nor the granting authority can be held responsible for them.

REFERENCES

[1] R. Abgrall, É. Le Mélédo, P. Öffner, and D. Torlo, *Relaxation deferred correction methods and their applications to residual distribution schemes*, The SMAI Journal of computational mathematics, 8 (2022), pp. 125–160.

[2] D. S. Balsara, *Self-adjusting, positivity preserving high order schemes for hydrodynamics and magnetohydrodynamics*, Journal of Computational Physics, 231 (2012), pp. 7504–7517.

[3] W. Bo and M. Shashkov, *Adaptive reconnection-based arbitrary Lagrangian Eulerian method*, Journal of Computational Physics, 299 (2015), pp. 902–939.

[4] W. Boscheri and M. Dumbser, *Arbitrary-Lagrangian-Eulerian one-step WENO finite volume schemes on unstructured triangular meshes*, Communications in Computational Physics, 14 (2013), pp. 1174–1206.

[5] W. Boscheri and M. Dumbser, *Arbitrary-Lagrangian–Eulerian discontinuous Galerkin schemes with a posteriori subcell finite volume limiting on moving unstructured meshes*, Journal of Computational Physics, 346 (2017), pp. 449–479.

[6] W. Boscheri, M. Tavelli, and L. Pareschi, *On the construction of conservative semi-lagrangian IMEX advection schemes for multiscale time dependent PDEs*, Journal of Scientific Computing, 90 (2022), p. 97.

[7] S. Busto, S. Chiocchetti, M. Dumbser, E. Gaburro, and I. Peshkov, *High order ADER schemes for continuum mechanics*, Frontiers in Physics, 8 (2020), p. 32.

[8] S. Busto and M. Dumbser, *A new family of thermodynamically compatible discontinuous Galerkin methods for continuum mechanics and turbulent shallow water flows*, Journal of Scientific Computing, 93 (2022), p. 56.

[9] S. Busto, M. Dumbser, C. Escalante, N. Favrie, and S. Gavrilyuk, *On high order ADER discontinuous Galerkin schemes for first order hyperbolic reformulations of nonlinear dispersive systems*, Journal of Scientific Computing, 87 (2021), p. 48.

[10] C. C. Castro and E. F. Toro, *Solvers for the high-order Riemann problem for hyperbolic balance laws*, Journal of Computational Physics, 227 (2008), pp. 2481–2513.

[11] M. Castro, J. Gallardo, J. López, and C. Parés, *Well-balanced high order extensions of godunov's method for semilinear balance laws*, SIAM Journal of Numerical Analysis, 46 (2008), pp. 1012–1039.

[12] M. Castro, J. Gallardo, and C. Parés, *High-order finite volume schemes based on reconstruction of states for solving hyperbolic systems with nonconservative products. Applications to shallow-water systems*, Mathematics of Computation, 75 (2006), pp. 1103–1134.
[13] S. Chiocchetti, I. Peshkov, S. Gavrilyuk, and M. Dumbser, *High order ADER schemes and GLM curl cleaning for a first order hyperbolic formulation of compressible flow with surface tension*, Journal of Computational Physics, 426 (2021), p. 109898.
[14] M. Ciallella, S. Clain, E. Gaburro, and M. Ricchiuto, *Very high order treatment of embedded curved boundaries in compressible flows: ADER discontinuous Galerkin with a space-time Reconstruction for Off-site data*, Computers & Mathematics with Applications, 175 (2024), pp. 1–18.
[15] B. Cockburn and C.-W. Shu, *The local discontinuous Galerkin method for time-dependent convection-diffusion systems*, SIAM journal on numerical analysis, 35 (1998), pp. 2440–2463.
[16] M. Dumbser, D. Balsara, E. Toro, and C.-D. Munz, *A unified framework for the construction of one-step finite volume and discontinuous Galerkin schemes on unstructured meshes*, Journal of Computational Physics, 227 (2008), pp. 8209–8253.
[17] M. Dumbser and M. Facchini, *A space-time discontinuous Galerkin method for Boussinesq-type equations*, Applied Mathematics and Computation, 272 (2016), pp. 336–346.
[18] M. Dumbser, F. Fambri, M. Tavelli, M. Bader, and T. Weinzierl, *Efficient implementation of ader discontinuous galerkin schemes for a scalable hyperbolic pde engine*, axioms, 7 (2018), p. 63.
[19] M. Dumbser, M. Käser, V. Titarev, and E. Toro, *Quadrature-free non-oscillatory finite volume schemes on unstructured meshes for nonlinear hyperbolic systems*, Journal of Computational Physics, 226 (2007), pp. 204–243.
[20] M. Dumbser and C. Munz, *Building blocks for arbitrary high order discontinuous Galerkin schemes*, Journal of Scientific Computing, 27 (2006), pp. 215–230.
[21] M. Dumbser, I. Peshkov, E. Romenski, and O. Zanotti, *High order ADER schemes for a unified first order hyperbolic formulation of continuum mechanics: viscous heat-conducting fluids and elastic solids*, Journal of Computational Physics, 314 (2016), pp. 824–862.
[22] M. Dumbser, I. Peshkov, E. Romenski, and O. Zanotti, *High order ADER schemes for a unified first order hyperbolic formulation of Newtonian continuum mechanics coupled with electro-dynamics*, Journal of Computational Physics, 348 (2017), pp. 298–342.
[23] M. Dumbser, O. Zanotti, E. Gaburro, and I. Peshkov, *A well-balanced discontinuous Galerkin method for the first–order Z4 formulation of the Einstein–Euler system*, Journal of Computational Physics, 504 (2024), p. 112875.
[24] F. Fambri, *Discontinuous Galerkin methods for compressible and incompressible flows on space–time adaptive meshes: toward a novel family of efficient numerical methods for fluid dynamics*, Archives of Computational Methods in Engineering, 27 (2020), pp. 199–283.
[25] F. Fambri, M. Dumbser, S. Köppel, L. Rezzolla, and O. Zanotti, *ADER discontinuous Galerkin schemes for general-relativistic ideal magnetohydrodynamics*, Monthly Notices of the Royal Astronomical Society, 477 (2018), pp. 4543–4564.
[26] E. G. Fernández, M. C. Díaz, M. Dumbser, and T. M. De Luna, *An arbitrary high order well-balanced ADER-DG numerical scheme for the multilayer shallow-water model with variable density*, Journal of Scientific Computing, 90 (2022), p. 52.
[27] L. Friedrich, G. Schnücke, A. R. Winters, D. C. D. R. Fernández, G. J. Gassner, and M. H. Carpenter, *Entropy stable space–time discontinuous Galerkin schemes with summation-by-parts property for hyperbolic conservation laws*, Journal of Scientific Computing, 80 (2019), pp. 175–222.
[28] E. Gaburro, *A unified framework for the solution of hyperbolic PDE systems using high order direct Arbitrary-Lagrangian–Eulerian schemes on moving unstructured meshes with topology change*, Archives of Computational Methods in Engineering, 28 (2021), pp. 1249–1321.
[29] E. Gaburro, *High order Well-Balanced Arbitrary-Lagrangian-Eulerian ADER discontinuous Galerkin schemes on general polygonal moving meshes*, Computers & Fluids, (2025), p. 106764.
[30] E. Gaburro, W. Boscheri, S. Chiocchetti, C. Klingenberg, V. Springel, and M. Dumbser, *High order direct Arbitrary-Lagrangian-Eulerian schemes on moving Voronoi meshes with topology changes*, Journal of Computational Physics, 407 (2020), p. 109167.
[31] E. Gaburro and S. Chiocchetti, *High-order Arbitrary-Lagrangian-Eulerian schemes on crazy moving Voronoi meshes*, in Young Researchers Conference, Springer, 2021, pp. 99–119.
[32] E. Gaburro and M. Dumbser, *A Posteriori Subcell Finite Volume Limiter for General PNPM*

Schemes: Applications from Gasdynamics to Relativistic Magnetohydrodynamics, Journal of Scientific Computing, 86 (2021), pp. 1–41.

[33] E. Gaburro, P. Öffner, M. Ricchiuto, and D. Torlo, *High order entropy preserving ADER-DG schemes*, Applied Mathematics and Computation, 440 (2023), p. 127644.

[34] G. Gassner, M. Dumbser, F. Hindenlang, and C. Munz, *Explicit one–step time discretizations for discontinuous Galerkin and finite volume schemes based on local predictors*, Journal of Computational Physics, 230 (2011), pp. 4232–4247.

[35] M. Han Veiga, L. Micalizzi, and D. Torlo, *On improving the efficiency of ADER methods*, Applied Mathematics and Computation, 466 (2024), p. 128426.

[36] M. Han Veiga, P. Öffner, and D. Torlo, *DeC and ADER: similarities, differences and a unified framework*, Journal of Scientific Computing, 87 (2021), p. 2.

[37] A. Hidalgo and M. Dumbser, *ADER schemes for nonlinear systems of stiff advection–diffusion–reaction equations*, Journal of Scientific Computing, 48 (2011), pp. 173–189.

[38] H. Jackson, *On the eigenvalues of the ADER-WENO Galerkin predictor*, Journal of Computational Physics, 333 (2017), pp. 409–413.

[39] M. Käser and A. Iske, *Adaptive ADER schemes for the solution of scalar non-linear hyperbolic problems*, J Comput Phys, 205 (2005), pp. 489–508.

[40] M. A. Käser, *Adaptive methods for the numerical simulation of transport processes*, PhD thesis, Technische Universität München, 2003.

[41] F. Kemm, E. Gaburro, F. Thein, and M. Dumbser, *A simple diffuse interface approach for compressible flows around moving solids of arbitrary shape based on a reduced Baer–Nunziato model*, Computers & fluids, 204 (2020), p. 104536.

[42] A. Lakiss, T. Heuzé, M. Tannous, and L. Stainier, *ADER discontinuous Galerkin material point method*, International Journal for Numerical Methods in Engineering, 125 (2024), p. e7365.

[43] R. J. LeVeque, *Finite difference methods for ordinary and partial differential equations: steady-state and time-dependent problems*, SIAM, 2007.

[44] Y. Liu, C.-W. Shu, E. Tadmor, and M. Zhang, *L2 stability analysis of the central discontinuous Galerkin method and a comparison between the central and regular discontinuous Galerkin methods*, ESAIM: Mathematical Modelling and Numerical Analysis, 42 (2008), pp. 593–607.

[45] F. Lörcher, G. Gassner, and C.-D. Munz, *A discontinuous Galerkin scheme based on a space–time expansion. I. Inviscid compressible flow in one space dimension*, Journal of Scientific Computing, 32 (2007), pp. 175–199.

[46] R. Loubère, P. H. Maire, M. Shashkov, J. Breil, and S. Galera, *ReALE: A reconnection-based arbitrary-Lagrangian–Eulerian method*, Journal of Computational Physics, 229 (2010), pp. 4724–4761.

[47] M. Marot-Lassauzaie and M. Bader, *Mixed-Precision in High-Order Methods: the Impact of Floating-Point Precision on the ADER-DG Algorithm*, arXiv preprint arXiv:2504.06889, (2025).

[48] S. May and M. Berger, *An explicit implicit scheme for cut cells in embedded boundary meshes*, Journal of Scientific Computing, 71 (2017), pp. 919–943.

[49] S. May and F. Laakmann, *Accuracy analysis for explicit-implicit finite volume schemes on cut cell meshes*, Communications on Applied Mathematics and Computation, 6 (2024), pp. 2239–2264.

[50] L. Micalizzi, D. Torlo, and W. Boscheri, *Efficient iterative arbitrary high-order methods: an adaptive bridge between low and high order*, Communications on Applied Mathematics and Computation, 7 (2025), pp. 40–77.

[51] S. Michel, D. Torlo, M. Ricchiuto, and R. Abgrall, *Spectral analysis of continuous FEM for hyperbolic PDEs: influence of approximation, stabilization, and time-stepping*, Journal of Scientific Computing, 89 (2021), p. 31.

[52] S. Michel, D. Torlo, M. Ricchiuto, and R. Abgrall, *Spectral analysis of high order continuous FEM for hyperbolic PDEs on triangular meshes: influence of approximation, stabilization, and time-stepping*, Journal of Scientific Computing, 94 (2023), p. 49.

[53] R. Millington, E. Toro, and L. Nejad, *Arbitrary High Order Methods for Conservation Laws I: The One Dimensional Scalar Case*, PhD thesis, Manchester Metropolitan University, Department of Computing and Mathematics, June 1999.

[54] S. Muzzolon, M. Dumbser, O. Zanotti, and E. Gaburro, *High order numerical discretizations of the Einstein-Euler equations in the generalized harmonic formulation*, arXiv preprint arXiv:2512.24121, (2025).

[55] P. Öffner, J. Glaubitz, and H. Ranocha, *Stability of correction procedure via reconstruction with summation-by-parts operators for Burgers' equation using a polynomial chaos*

approach, ESAIM: Mathematical Modelling and Numerical Analysis, 52 (2018), pp. 2215–2245.

[56] P. Öffner, L. Petri, and D. Torlo, *Analysis for implicit and implicit-explicit ADER and DeC methods for ordinary differential equations, advection-diffusion and advection-dispersion equations*, Applied Numerical Mathematics, 212 (2025), pp. 110–134.

[57] C. Parés, *Numerical methods for nonconservative hyperbolic systems: a theoretical framework*, SIAM Journal on Numerical Analysis, 44 (2006), pp. 300–321.

[58] I. Popov, *Space-Time Adaptive ADER-DG Finite Element Method with LST-DG Predictor and a posteriori Sub-cell WENO Finite-Volume Limiting for Simulation of Non-stationary Compressible Multicomponent Reactive Flows*, Journal of Scientific Computing, 95 (2023), p. 44.

[59] I. S. Popov, *The effective use of BLAS interface for implementation of finite-element ADER-DG and finite-volume ADER-WENO methods*, arXiv preprint arXiv:2409.12483, (2024).

[60] I. S. Popov, *High order ADER-DG method with local DG predictor for solutions of differential-algebraic systems of equations*, Journal of Scientific Computing, 102 (2025), p. 48.

[61] I. S. Popov, *Theory and internal structure of ADER-DG method for ordinary differential equations*, arXiv preprint arXiv:2508.13824, (2025).

[62] J. Qiu, M. Dumbser, and C. Shu, *The discontinuous Galerkin method with Lax-Wendroff type time discretizations*, Computer Methods in Applied Mechanics and Engineering, 194 (2005), pp. 4528–4543.

[63] L. Rannabauer, M. Dumbser, and M. Bader, *ADER-DG with a-posteriori finite-volume limiting to simulate tsunamis in a parallel adaptive mesh refinement framework*, Computers & Fluids, 173 (2018), pp. 299–306.

[64] H. Ranocha, M. Sayyari, L. Dalcin, M. Parsani, and D. I. Ketcheson, *Relaxation Runge–Kutta methods: Fully discrete explicit entropy-stable schemes for the compressible Euler and Navier–Stokes equations*, SIAM Journal on Scientific Computing, 42 (2020), pp. A612–A638.

[65] K. Ricardo and K. Duru, *Scalable ADER-DG transport method with polynomial order independent CFL limit*, arXiv preprint arXiv:2507.07304, (2025).

[66] L. Río-Martín and M. Dumbser, *High-order ADER Discontinuous Galerkin schemes for a symmetric hyperbolic model of compressible barotropic two-fluid flows*, Communications on Applied Mathematics and Computation, 6 (2024), pp. 2119–2154.

[67] V. V. Rusanov, *Calculation of Interaction of Non–Steady Shock Waves with Obstacles*, J. Comput. Math. Phys. USSR, 1 (1961), pp. 267–279.

[68] S. Sherwin, *Dispersion analysis of the continuous and discontinuous Galerkin formulations*, in Discontinuous Galerkin Methods: Theory, Computation and Applications, Springer, 2000, pp. 425–431.

[69] M. Tavelli, S. Chiocchetti, E. Romenski, A.-A. Gabriel, and M. Dumbser, *Space-time adaptive ADER discontinuous Galerkin schemes for nonlinear hyperelasticity with material failure*, Journal of computational physics, 422 (2020), p. 109758.

[70] V. Titarev and E. Toro, *ADER: Arbitrary high order Godunov approach*, Journal of Scientific Computing, 17 (2002), pp. 609–618.

[71] E. Toro, R. Millington, and L. Nejad, *Towards very high order Godunov schemes*, in Godunov Methods. Theory and Applications, E. Toro, ed., Kluwer/Plenum Academic Publishers, 2001, pp. 905–938.

[72] E. Toro and V. Titarev, *Solution of the generalized Riemann problem for advection-reaction equations*, Proc. Roy. Soc. London, 458 (2002), pp. 271–281.

[73] S. Wolf, A.-A. Gabriel, and M. Bader, *Optimization and local time stepping of an ader-dg scheme for fully anisotropic wave propagation in complex geometries*, in International Conference on Computational Science, Springer, 2020, pp. 32–45.

[74] J. Yan and C.-W. Shu, *A local discontinuous galerkin method for kdv type equations*, SIAM Journal on Numerical Analysis, 40 (2002), pp. 769–791.

[75] J. Yan and C.-W. Shu, *Local discontinuous galerkin methods for partial differential equations with higher order derivatives*, Journal of Scientific Computing, 17 (2002), pp. 27–47.

[76] D. Yuan, P. Tsoutsanis, and K. Jenkins, *Hybrid high-order finite volume discontinuous Galerkin methods for turbulent flows*, in World Congress in Computational Mechanics and ECCOMAS Congress, 2022.

[77] O. Zanotti, M. Dumbser, D. Balsara, and D. Bhoriya, *A new first-order formulation of the Einstein equations: comparison among different high order numerical schemes*, in Journal of Physics: Conference Series, vol. 2997, IOP Publishing, 2025, p. 012015.